Effect of Sulfur in Steel on Transient Evolution of Inclusions During Calcium Treatment

YANG LIU, LIFENG ZHANG, YING ZHANG, HAOJIAN DUAN, YING REN, and WEN YANG

In the current study, the effect of S content in the molten steel on inclusions during calcium treatment was studied using an induction furnace. The calcium in steel decreased from 48 to 2 ppm, and the sulfur in steel changed a little with time. When sulfur content in steel was as low as 25 ppm during calcium treatment, inclusions shifted from CaO-Al_2O_3-CaS to Al_2O_3-CaO with about 35 pct CaO. When the sulfur increased over 90 ppm, more CaS-CaO formed just after the addition of calcium, and then the CaS content decreased from over 45 pct to lower than 15 pct and inclusions were mostly Al_2O_3-CaO-CaS and Al_2O_3-CaO with a high Al_2O_3 content. Thermodynamic calculation predicted the variation of the composition of inclusions, indicating good agreement with the measurement, while a certain deviation existed, especially for heats with 90 and 180 ppm sulfur. A reaction model was proposed for the formation of CaO and CaS, which considered the reaction between calcium vapor bubbles in the zone and the dissolved oxygen and sulfur in the molten steel, as described by a Langmuir-type adsorption isotherm with a reaction occurring on the remaining vacant sites. The variation of transient CaS inclusions was discussed based on the thermodynamic calculation and the morphology evolution of typical inclusions containing CaS.

https://doi.org/10.1007/s11663-018-1179-x

I. INTRODUCTION

THE major objectives of calcium treatment in the steel secondary refining process include (1) to diminish nozzle clogging and to improve castability by controlling the composition of inclusions[1-4] and (2) to improve the product property of the steel by controlling the shape of inclusions.[5-7] Excessive or insufficient addition of calcium can bring adverse effects. The excessive addition of calcium is detrimental to castability due to the formation of solid CaS inclusions[8-11] and the reaction between the redundant calcium in the molten steel and the alumina containing in the slag or in the refractory, which lowers the cleanliness of the steel.[12,13] If an insufficient amount of calcium is added, inclusions are hardly modified to target liquid ones so that the castability is hardly improved.[8-10] Hence, the composition of inclusions, such as CaO, CaS, and Al_2O_3, should be well controlled in order to obtain the desired properties of steel.[14] Thermodynamic calculation was extensively performed to accurately predict the composition of inclusions considering the effect of the dissolved aluminum ($[Al]_s$), the sulfur, the total calcium (T.Ca), and the total oxygen (T.O.) in steels.[8,12,15-17]

Sulfur in the molten steel has a significant effect on inclusions during calcium treatment.[13,18-25] The formation of CaS easily occurred in steels with high sulfur and aluminum contents.[26] The generation of CaS prevented calcium from reacting with Al_2O_3 when the sulfur content was high in the molten steel.[4,24,27,28] Lu *et al.*[29] and Verma *et al.*[30] proposed that the extent of calcium capture depended on the sulfur content in the steel. Formation and evolution mechanisms of CaS can be summarized as follows: (1) inclusions of CaS are generated as transient phase[29-31] immediately upon calcium injection and then decompose due to the evaporation of calcium,[32] as shown in Reaction [1]; (2) inclusions of CaS form as a transient phase and then react with the alumina to yield modified inclusions by Reaction [2];[30,31,33,34] (3) inclusions of CaO-Al_2O_3-CaS form first and then convert to CaS-Al_2O_3 inclusions in steels with low T.O. and high sulfur contents since the reaction between CaO and dissolved S occurs, as shown in Reaction [3];[35] and (4) inclusions of CaS precipitate in the generated CaO-CaS-Al_2O_3 inclusions due to the reverse reaction of Eq. [2].[28] In the equations, symbol [ ] denotes an element dissolved in steel melt, () denotes a

YANG LIU, LIFENG ZHANG, YING ZHANG, HAOJIAN DUAN, YING REN, and WEN YANG are with the School of Metallurgical and Ecological Engineering, University of Science and Technology Beijing (USTB), Beijing 100083, People's Republic of China. Contact e-mail: zhanglifeng@ustb.edu.cn
Manuscript submitted July 4, 2017.
Article published online January 30, 2018.

component dissolved in liquid slag inclusions, and subscript "inc" denotes a solid (saturation) phase.[20]

$$(CaS)_{inc} = [Ca] + [S] \quad [1]$$

$$3(CaS)_{inc} + (Al_2O_3)_{inc} = 3(CaO)_{inc} + 2[Al] + 3[S] \quad [2]$$

$$(CaO)_{inc} + [S] = (CaS)_{inc} + [O] \quad [3]$$

The existence types of CaS inclusions during calcium treatment are listed as follows: (1) in contact with an oxide inclusion,[2,36,37] (2) surrounding an oxide inclusion as an outside layer as a ring,[1,38-40] (3) uniformly distributed within oxides,[27] (4) pure one,[13,30] and (5) (Ca,Mn)S type.[36,41] For the first three types, the formation of complex inclusions is attributed to the transient formation, precipitation, and reaction of CaS, respectively.[27] For the stable CaS, it forms in steel with high sulfur or with excessive calcium addition.[30] For the (Ca,Mn)S type, CaS and MnS can dissolve each other to generate a solid solution.[39,41-43] However, the formation of CaO and CaS just after the addition of calcium was little investigated.

In the current study, laboratory scale experiments for the modification of inclusions by calcium treatment in electrolytic iron were performed using a vacuum induction furnace, which favors the control of oxygen and sulfur in steels. Characteristics of inclusions in steel samples taken at various times were investigated to study the effect of sulfur on the transient evolution of inclusions. Thermodynamic prediction was performed using Factsage 7.0 software.* A reaction model was proposed for the formation of CaS and CaO. The variation of transient CaS inclusions was discussed based on the thermodynamic calculation and the morphology evolution of typical inclusions containing CaS.

*FACTSAGE is a trademark of ThermFact LTD, Montreal, Canada and GTT-Technologies, Herzogenrath, Germany.

II. EXPERIMENTAL METHODOLOGY

In the current study, in order to study the effect of sulfur on inclusions in the molten steel during calcium treatment, experiments were performed in an alumina crucible with electrolytic iron containing 25 to 180 ppm sulfur. A 20-kW vacuum induction furnace was employed for steel melting, alloy addition, and sampling. The schematic of the experimental apparatus is shown in Figure 1. Five samplers were installed in the sampling box and each could move vertically in order to add alloy and take samples. The pipe sampler could be switched by rotating the flange outside. The Ca-Si powders (30 pct Ca-70 pct Si) were wrapped with an iron foil and tied to a molybdenum rod fixed in the bottom of a sampler. The other four samplers were silica

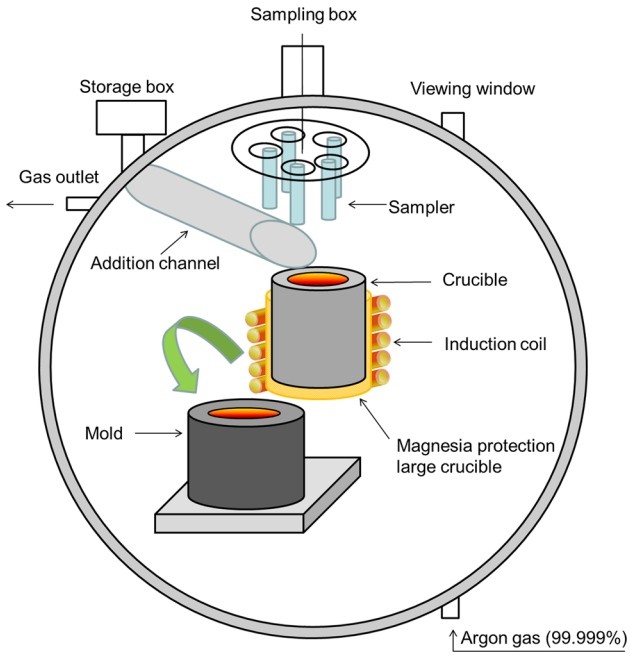

Fig. 1—Schematic of the experimental apparatus.

tubes. The chamber was evacuated with a mechanical pump to a vacuum lower than 10 Pa and then backfilled with a high-purity argon gas. This procedure was repeated twice to decrease the oxygen pressure in the chamber followed by backfilling with the high-purity argon to atmospheric pressure to avoid reoxidation. The temperature of the melt was measured during the experiment with a dual-wavelength pyrometer through a top window. The temperature calibration was carried out in advance by comparing measured values with the measured ones with a platinum rhodium thermocouple as a reference. For each experiment, 700-g electrolytic iron was melted and the molten steel was held for 2 minutes in 1873 K (1600 °C) with the chemical composition shown in Table I. Then 1.1 g Fe_2O_3 powder, 1 g pure Al (99.999 pct), and a certain amount of FeS powder (0, 0.085, 0.18, and 0.4 g, respectively) were added into the melt from the storage box through the addition channel. Two minutes later, 4 g CaSi powder (30 pct Ca-70 pct Si) was inserted into the molten steel for calcium treatment. Samples were taken after the addition of calcium at 1, 3, 5, and 7 minutes, and the melt was poured into an iron mold at 10 minutes, as shown in Figure 2.

For each sample, a cross section 8 mm from the bottom of the sample was used to detect inclusions, and this location was chosen based on previous results.[30] Steel powders were machined from the other part of samples to measure contents of the T.Ca, the $[Al]_s$, and the total sulfur (T.S.) in the steel, and a 5-mm-diameter rod was machined from the sample to test T.O. and N content. For the last tapped sample, the horizontal cross section position 15 mm from the bottom was scanned to find the size, morphology, and composition of inclusions using an ASPEX PSEM EXPLORER (FEI Corporation, Hillsboro, OR) with an automated Feature Analysis

Table I. Chemical Composition of the Electrolytic Iron Used in the Current Study (Mass ppm)

C	S	P	Si	Mn	Cr	T.O.	Al	Mg	Ca
5	6	4	5	1	5	70	18	4	1

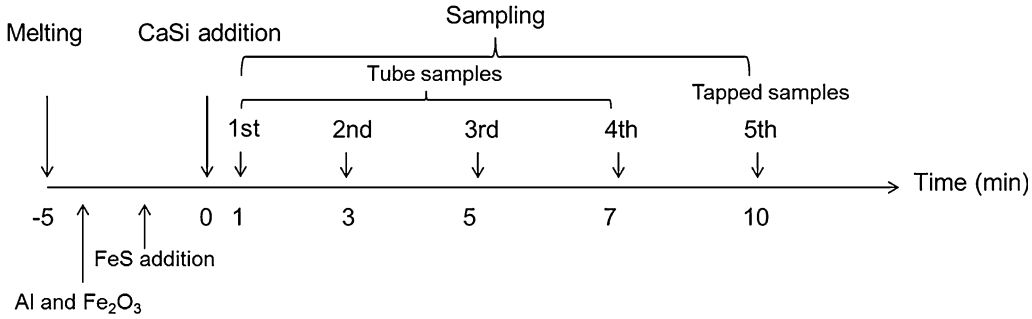

Fig. 2—Addition of alloys and sampling procedure in the current experiments.

system. The scanning area was 20 to 30 mm^2 in order to catch hundreds of inclusions. The composition of the steel was measured with an inductively coupled plasma optical emission spectrometer (model 725ES; ICP-725ES, Varian Inc., Palo Alto City, CA) and the nitrogen and oxygen were analyzed with a LECO** analyzer (model TCH600).

**LECO is a trademark of LECO Corporation, St. Joseph, MI.

III. CHARACTERIZATION OF INCLUSIONS IN STEEL

The $[Al]_s$, T.Ca, T.O., and T.S. contents in steel samples are listed in Table II. For each heat, the T.Ca content increased first after the addition of Ca-Si alloys and then decreased from 48 to 2 ppm. Based on the measured calcium content in the 1-minute sample, the yielding rate of calcium was about 3 pct. The T.O. content fluctuated in the range of 9.7 to 29.2 ppm in steel samples taken at different times. The variation of the T.O. and the T.Ca has been studied in another article and will not be discussed here.[44] The contents of $[Al]_s$ and T.S. changed little during each experiment. As fundamental research on calcium treatment in laboratory experiments, Al content in the current study is higher than that in the Al-killed steels in the plant trial. The experiments with lower Al content will be performed in our future study and the comparison will be made with current results.

The sulfur content of the steel has a significant effect on the composition of inclusions during calcium treatment. In the current study, CaO, CaS, and Al_2O_3 are mass fractions in the ternary diagrams. When the sulfur content in steel was as low as 25 ppm (heat A), at 1- and 3-minute samples, the measured inclusions were mostly CaO-Al_2O_3 and CaO-Al_2O_3-CaS. Just after the addition of calcium, some inclusions were CaS-CaO-Al_2O_3 with a high content of CaS, while more inclusions were CaO-Al_2O_3 with low CaS contents due to the limited sulfur content. Hence, the average composition in the 1-minute sample is close to that in the 3-minute sample. With increased time, inclusions shifted to CaO-Al_2O_3 with low CaS content near the low melting point region, as shown in Figure 3. Each solid circle represented an inclusion and its size and color were in proportion to the real size of inclusions. Similar evolution of inclusions was observed in heat B. When the sulfur content increased to 90 ppm (heat C), inclusions were mostly CaS-CaO, CaS-Al_2O_3, and CaO-Al_2O_3-CaS at 1 minute. Inclusions of CaS-CaO were transferred to CaO -CaS-Al_2O_3 at 3 minutes, and inclusions were mostly Al_2O_3-CaS-CaO with a high Al_2O_3 content in the end. When sulfur content in steel increased to 180 ppm (heats D and E), the evolution of inclusions was similar to that in heat C, while CaS-CaO shifted to CaO-CaS-Al_2O_3 after 5 minutes.

Figures 4 and 5 show the composition and the size of inclusions in the Al_2O_3-CaS-CaO ternary system in steel with 90 and 180 ppm sulfur content. The variation of the composition of inclusions highly depends on the formation and the decomposition of CaS, which will be discussed in Sections IV and V of the current article.

Figure 6 shows the variation of the average composition of inclusions. The experiment with 180 ppm S was repeated in the current study. The different values of CaS, CaO, and Al_2O_3 in the two groups were attributed to different T.O. contents in steels. At the 1-minute sample, the CaS content was approximately 21.5, 34.8, 47, 56, and 60 pct for heats A, B, C, D, and E, respectively. As time goes by the CaS content decreased in each heat. For the low sulfur heat (heat A), the CaO content in inclusions was higher than 30 pct at each sample and slightly decreased at the last tapped sample. The CaO content decreased with the increase of sulfur content in steel. In high sulfur heats (heat D and E), the CaO content in inclusions was higher during the first 0 to 3 minutes than that in medium sulfur heats (heat B and C), while it decreased and was lower than 10 pct from 5 to 10 minutes. The Al_2O_3 content increased gradually with time in the low sulfur heat (heat A).

Table II. Composition of Steel Samples

	$[Al]_s$ (Pct)	T.Ca (ppm)	T.O. (ppm)	T.S. (ppm)
S = 25 ppm heat A				
1st sample	0.1	47	27.1	26
2nd sample	0.097	30	22.5	24
3rd sample	0.098	20	19.9	25
4th sample	0.093	7	18.8	24
Final sample	0.1	5	13.7	25
S = 50 ppm heat B				
1st sample	0.1	47	10.8	50
2nd sample	0.1	28	11.7	50
3rd sample	0.097	10	10.5	51
Final sample	0.096	5	12.6	52
S = 90 ppm heat C				
1st sample	0.086	43	14	90
2nd sample	0.086	26	18.3	89
3rd sample	0.088	11	19.7	91
4th sample	0.086	8	16.2	94
Final sample	0.092	2	13.9	91
S = 180 ppm heat D				
1st sample	0.1	48	12.6	179
2nd sample	0.1	22	12.2	183
3rd sample	0.098	14	16	183
4th sample	0.094	7	23.4	183
Final sample	0.092	4	15.5	189
S = 180 ppm heat E				
1st sample	0.1	47	12.3	177
2nd sample	0.1	14	9.7	171
3rd sample	0.1	12	15.5	183
4th sample	0.092	8	29.2	185
Final sample	0.1	3	12.8	191

Given the high sulfur content in steel in heats B, C, D, and E, the Al_2O_3 content was low at first due to the formation of CaS, while it increased sharply with time since the contents of CaS and CaO decreased. The Al_2O_3 content in inclusions was more than 75 pct at the last tapped sample, whereas it was lower than 65 pct in the low sulfur heat (heat A).

Figures 7 through 9 illustrate two-dimensional composition mappings of typical inclusions. For the low sulfur heat, for samples taken from 1 to 3 minutes, a dual-phased morphology of CaS adhering to $CaO\text{-}Al_2O_3$ or Al_2O_3 was observed, and $CaO\text{-}Al_2O_3$ inclusions with a CaS ring were also found, as shown in Figures 7(a) and (b). For samples taken from 5 to 10 minutes, inclusions were mostly $CaO\text{-}Al_2O_3$ and a certain amount of $CaO\text{-}CaS\text{-}Al_2O_3$ complex inclusions also existed, as shown in Figures 7(c) through (e). For the medium sulfur heats, for a sample at 1 minute, inclusions were mostly $CaS\text{-}CaO\text{-}Al_2O_3$ and $CaS\text{-}Al_2O_3$. Calcium alumina inclusions were completely or annularly surrounded with CaS, and a certain content of CaS attached to Al_2O_3 was also found, as shown in Figures 8(a) and (b). For samples taken after 3 and 5 minutes, inclusions shifted to $CaO\text{-}CaS\text{-}Al_2O_3$ and $CaS\text{-}Al_2O_3$, and inclusions were mostly $CaO\text{-}Al_2O_3$ in the core surrounded with CaS, as shown in Figures 8(c) and (d). At the 7-minute sample and the tapped sample, inclusions were $CaO\text{-}Al_2O_3$ with a little CaS and $CaO\text{-}CaS\text{-}Al_2O_3$ complex ones, as shown in Figures 8(e) and (f). For high sulfur heats, for the 1-minute sample, inclusions were similar to those in heat C, while Al_2O_3 inclusions mostly attached to CaS and were little surrounded by CaS, as shown in Figure 9(a). Inclusions were transferred to $CaO\text{-}CaS\text{-}Al_2O_3$ and $CaS\text{-}Al_2O_3$ with time. Inclusions of $CaO\text{-}Al_2O_3$ were surrounded with CaS, and dual-phased inclusions containing CaS were also found, as shown in Figures 9(b) and (c). Finally, inclusions shifted to uniform $CaO\text{-}CaS\text{-}Al_2O_3$ or $CaO\text{-}Al_2O_3$ with a high Al_2O_3 content, as shown in Figures 9(d) and (e).

IV. FORMATION MECHANISM OF CALCIUM OXIDE AND CALCIUM SULFIDE

The evaporation of calcium during calcium treatment of steel has been reported. After the addition of Ca-Si powders, the reaction between the dissolved calcium and the dissolved oxygen and sulfur in steel occurred so that CaO and CaS are formed. The contents of CaO and CaS in inclusions decreased gradually since the dissolved calcium vaporized and decreased in steel with the lapse of time.[32] The composition of inclusions depended highly on the sulfur content in the molten steel since the formation and decomposition reactions of CaS occurred. In the current study, the formation and evolution of CaS were discussed. Thermodynamic calculation was performed using Factsage 7.0 software with the FactPS, FToxid, and FTmisc databases. In the induction furnace, the quasi-equilibrium state could be

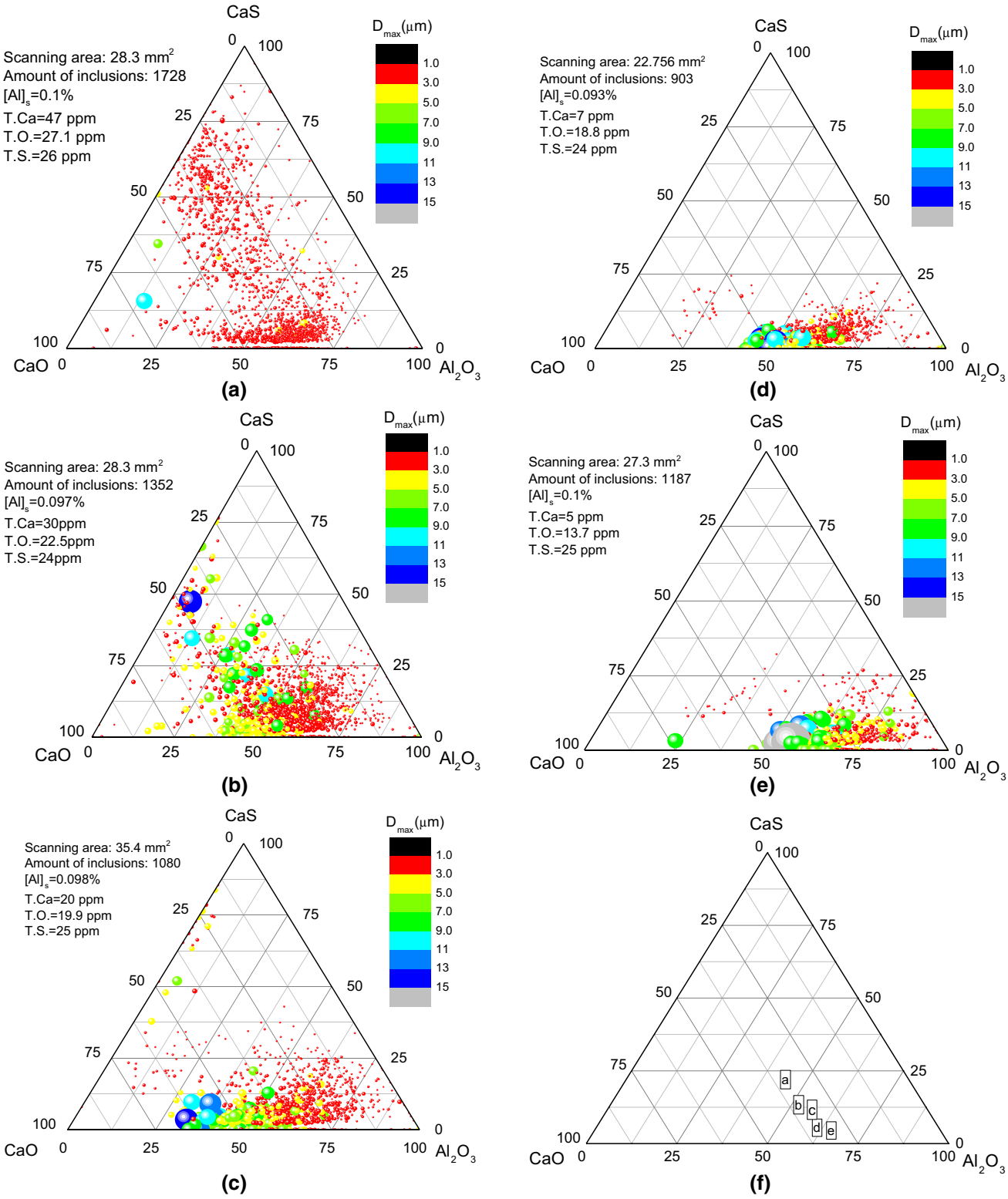

Fig. 3—Distribution of size and composition of inclusions in the Al_2O_3-CaS-CaO ternary phase diagram in Heat A (T.S. = 25 ppm) at (*a*) 1 min, (*b*) 3 min, (*c*) 5 min, (*d*) 7 min, (*e*) 10 min, and (*f*) average composition.

achieved in each stage due to favorable kinetic conditions. Hence, the thermodynamic calculation could predict the evolution tendency of the composition of inclusions.

Based on the calculated results with Factsage 7.0 software, with 10 ppm T.O. and 0.1 pct $[Al]_s$ in steel, the variation of the composition of inclusions with the contents of calcium and sulfur in steel is illustrated in

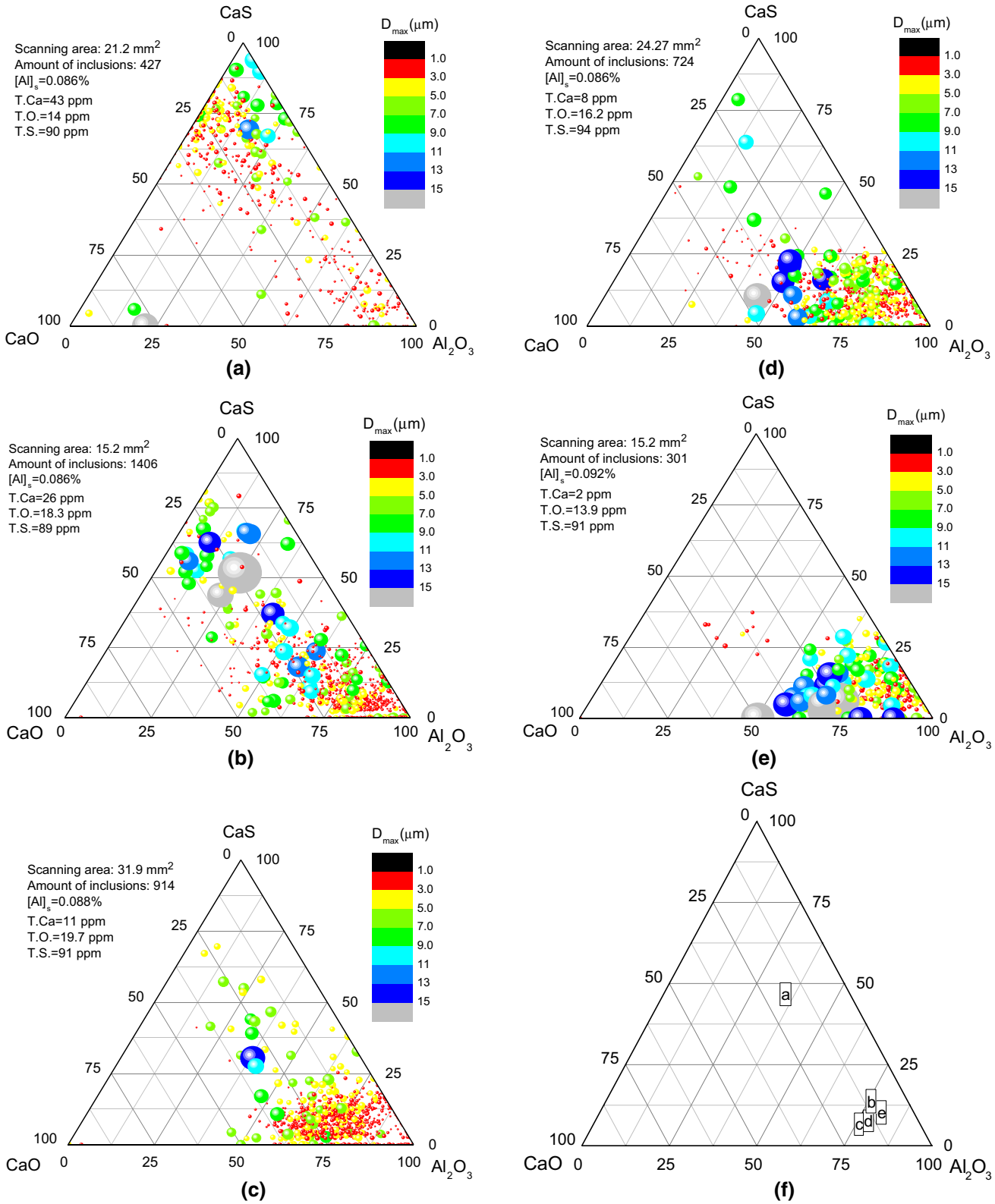

Fig. 4—Distribution of size and composition of inclusions in the Al_2O_3-CaS-CaO ternary phase diagram in Heat C (T.S. = 90 ppm) at (*a*) 1 min, (*b*) 3 min, (*c*) 5 min, (*d*) 7 min, (*e*) 10 min, and (*f*) average composition.

Figure 10. With the decreased calcium in steel, inclusions were transferred from CaS-CaO-Al_2O_3 to CaO-Al_2O_3, and then to (CaO)-Al_2O_3 finally. The formation of CaS-CaO-Al_2O_3 inclusions with a high Al_2O_3 content was favored in steel with high sulfur content. Figure 11 shows the critical condition for the

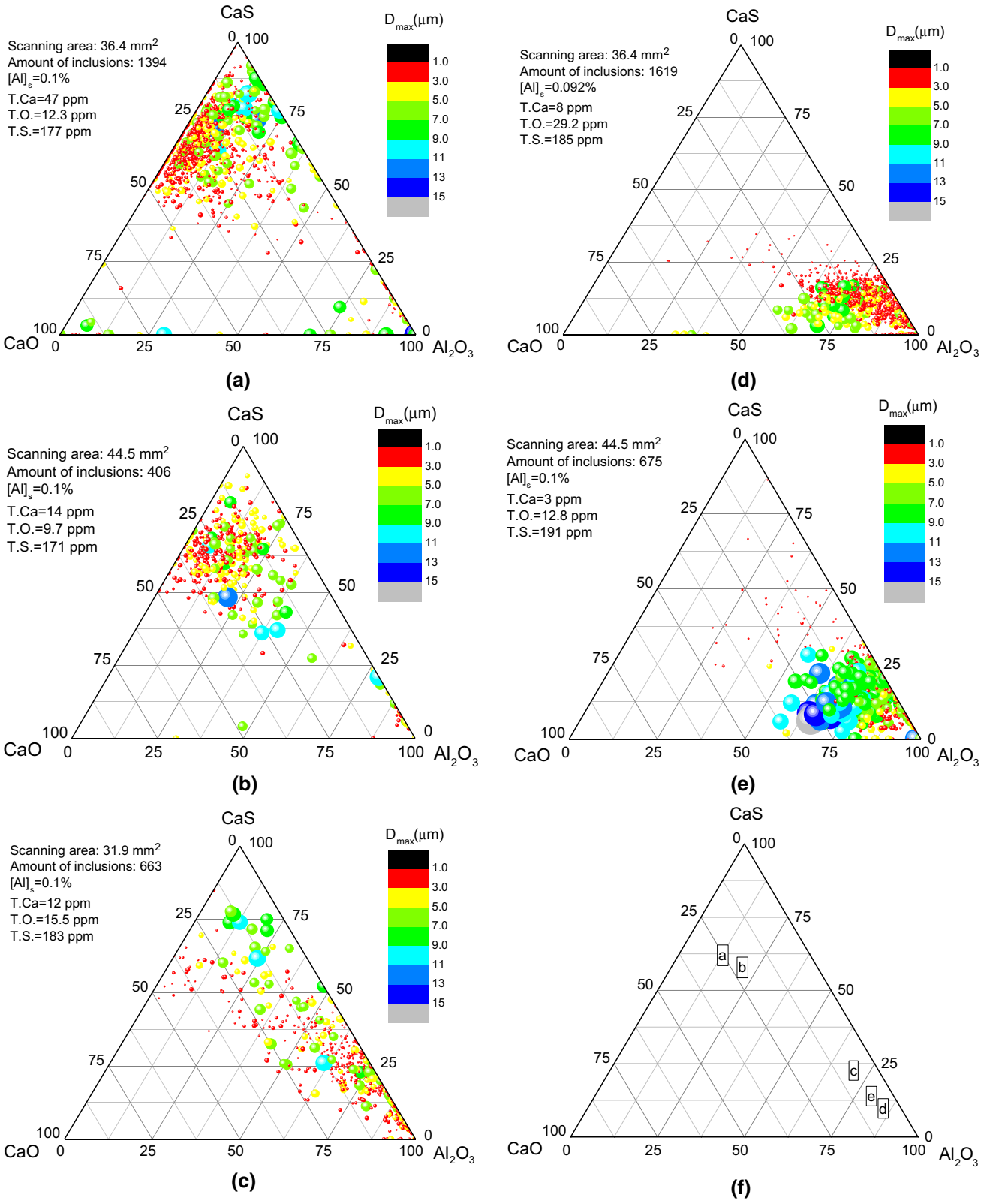

Fig. 5—Distribution of size and composition of inclusions in the Al_2O_3-CaS-CaO ternary phase diagram in Heat E (T.S. = 180 ppm) at (*a*) 1 min, (*b*) 3 min, (*c*) 5 min, (*d*) 7 min, (*e*) 10 min, and (*f*) average composition.

formation of CaS. The decomposition of CaS was favored by the evaporation of the dissolved calcium and the increase of the T.O. in steel.[44] The formation and decomposition of transient CaS inclusions had a significant influence on the composition of inclusions during calcium treatment.

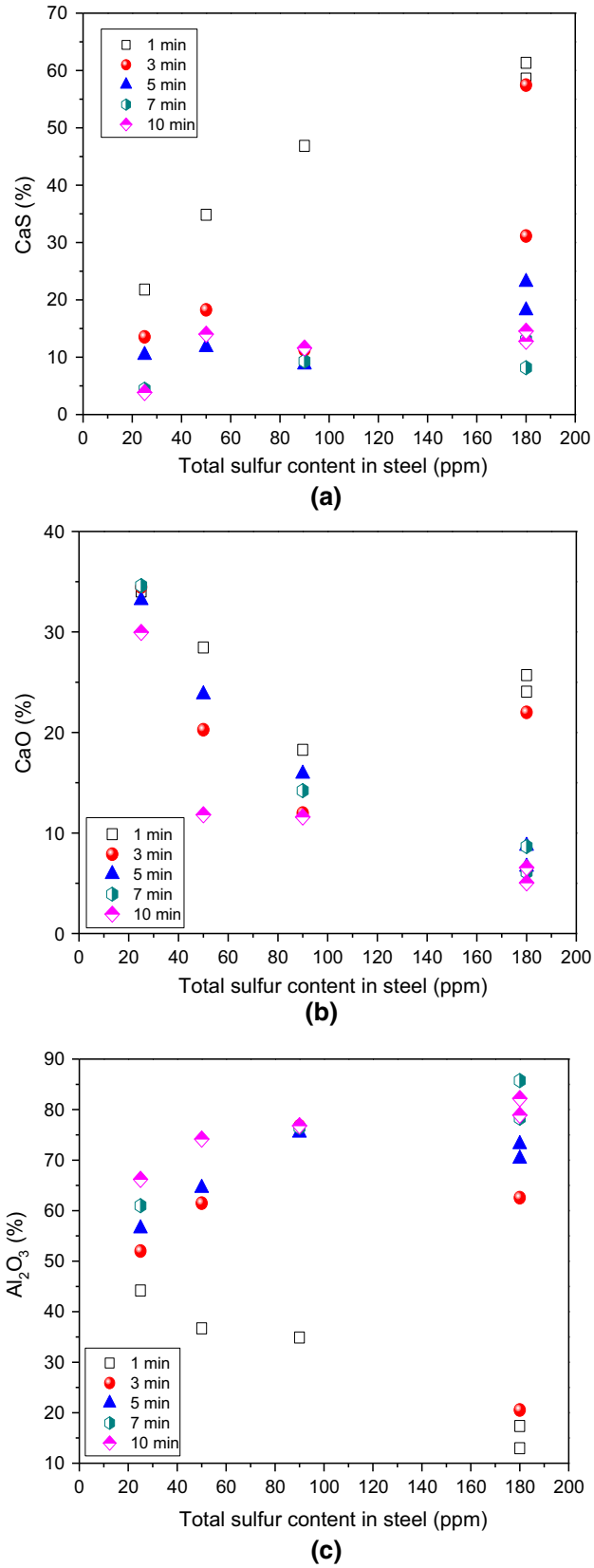

Fig. 6—Variation of (*a*) CaS, (*b*) CaO, and (*c*) Al_2O_3 content of inclusions with time.

Based on the composition of inclusions shown in Figures 3 through 5, the calculated variation of the composition of inclusions agreed with the measurement with a certain deviation. When Ca-Si powders were just added into the molten steel, a complete thermodynamic equilibrium could hardly be reached. Hence, it was hard to accurately predict the transient phenomena by thermodynamic calculation. In the current study, a reaction model was proposed for the formation of CaO and CaS just after the addition of calcium.

When calcium is added into the molten steel, the competition between oxygen and sulfur for available calcium, whether at the surface of calcium vapor bubbles or dissolved in the steel, could have an effect on the formation of CaO and CaS.[30] A calcium-rich zone exists in the molten steel just after the addition of calcium. The reaction between calcium vapor bubbles in the zone and the dissolved oxygen and sulfur in the molten steel could occur like the chemisorption of the dissolved solute, as described by a Langmuir-type adsorption isotherm with a reaction occurring on the remaining vacant sites, as shown in Figure 12. The formation of CaO and CaS molecules was assumed fast enough so that it would hardly hinder the next absorption for oxygen and sulfur to the surface of calcium vapor. The progress would be ongoing until the calcium vapor was consumed completely or evaporated from the surface of the melt to the atmosphere. The components of CaS and CaO became detectable by the agglomeration of smaller CaS and CaO particles. Thus, the dependence of the ratio on the surface constitution was described by a simple site coverage model in the monolayer approximation;[45] *i.e.*, the coverage of sulfur and oxygen was in proportion to their molar quantities in inclusions. For ideal Langmuir adsorption,[46]

$$\frac{\theta_i}{1-\theta_i} = K_i a_i \qquad [4]$$

where θ is the fractional coverage by the single solute i, a_i is the activity, and K is the equilibrium constant.

For the case of many ideally adsorbed interfering solute elements, the equation could be written as

$$\frac{\theta_i}{1-\sum_j \theta_j} = K_i a_i \qquad [5]$$

Relative extents of sulfur and oxygen segregation to the interface between liquid steel and gas (such as calcium vapor) were estimated using the literature data on surface segregation with segregation constants of $K_O = 300$ and $K_S = 130$ for oxygen and sulfur, respectively, according to the previous equation containing oxygen with a Henrian activity of 4.6 ppm (from the Al-O equilibrium diagram) and variable sulfur.[30,45] Oxygen and sulfur contents in CaO and CaS were calculated based on the measured mass fractions of CaO and CaS in inclusions. By assuming the measured average diameter to be equal to the real diameter of each inclusion, elements of calcium, oxygen, and sulfur

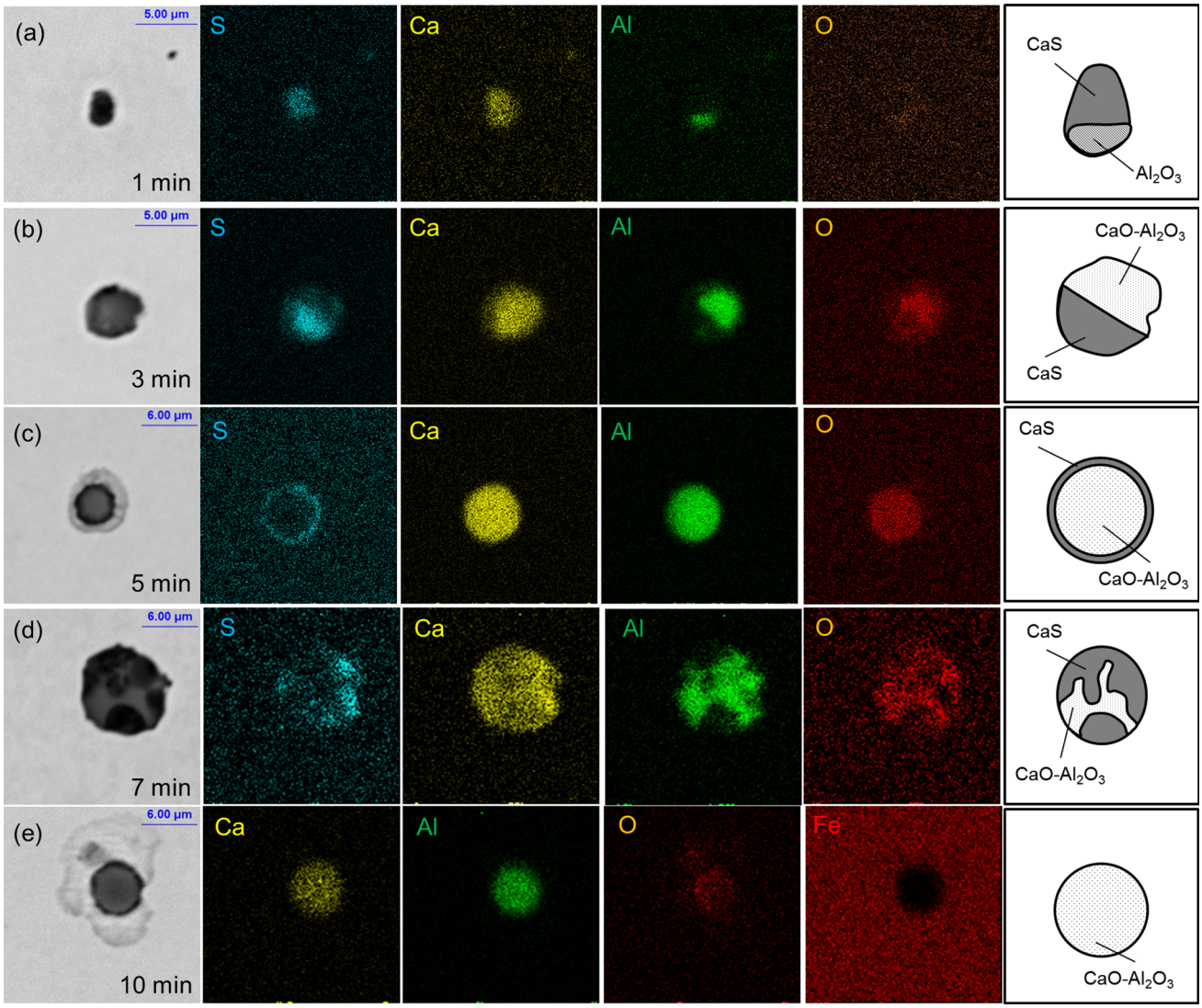

Fig. 7—Typical inclusions in steel with 25 ppm sulfur: (*a*) CaS-Al_2O_3, (*b*) complex CaS-CaO-Al_2O_3, (*c*) CaO-Al_2O_3 with a CaS ring, (*d*) CaO-Al_2O_3 surrounded by CaS, and (*e*) uniform CaO·Al_2O_3.

in detected inclusions as fractions of the total steel mass were calculated with the assumption of an average density of 3.5 g/cm^3 for inclusions and 7.85 g/cm^3 for the steel.[30] Thus, calcium, oxygen, and sulfur contents in CaO and CaS inclusions and the molar ratio of S/(S + O) were obtained, as shown in Table III.

The concentration of the dissolved calcium in the steel is estimated to be a few parts per million at most,[47] while the excessive calcium content over 20 ppm[14,33] exists in the molten steel just after the addition of calcium, which is estimated by substracting the calcium content fixed in CaO and CaS from the T.Ca. Thus, the ratio of sulfur and oxygen in inclusions containing calcium in the 1-minute sample of each heat was investigated, whose variation tendency was in line with that of the calculated one using the Langmuir model, as shown in Figure 13. The measured result was lower than the calculated one since the reaction between CaS molecules and the atoms of the dissolved oxygen in steel occurred after CaS formed. When excessive calcium content existed in the molten steel, the rate of CaS formation was higher than that of CaS decomposition. The measured CaS content in inclusions was the resultant from the formation and decomposition of CaS inclusions. In the model, CaS decomposition was ignored since the decomposition rate of CaS is hard to test.

The relationship between the sulfur content in steels and the fraction of CaS decomposition is illustrated in Figure 14. For the sample taken at the same time in each heat, CaS decomposition highly depended on the reaction between CaS and [O]. Based on the chemical composition of the steel ([O] = 4.6 ppm, [Al] = 0.1 pct) and thermodynamic parameters listed in Table IV,[48,49] the change of Gibbs free energies (ΔG_r) of Reaction [3] with sulfur contents in steel was calculated by Eqs. [6] through [8], shown in Figure 15. In the current study, for the 1-minute sample of each heat, the dissolved calcium was approximately 30 to 40 ppm, and the dissolved sulfur content was approximately equal to the total one before calcium addition.

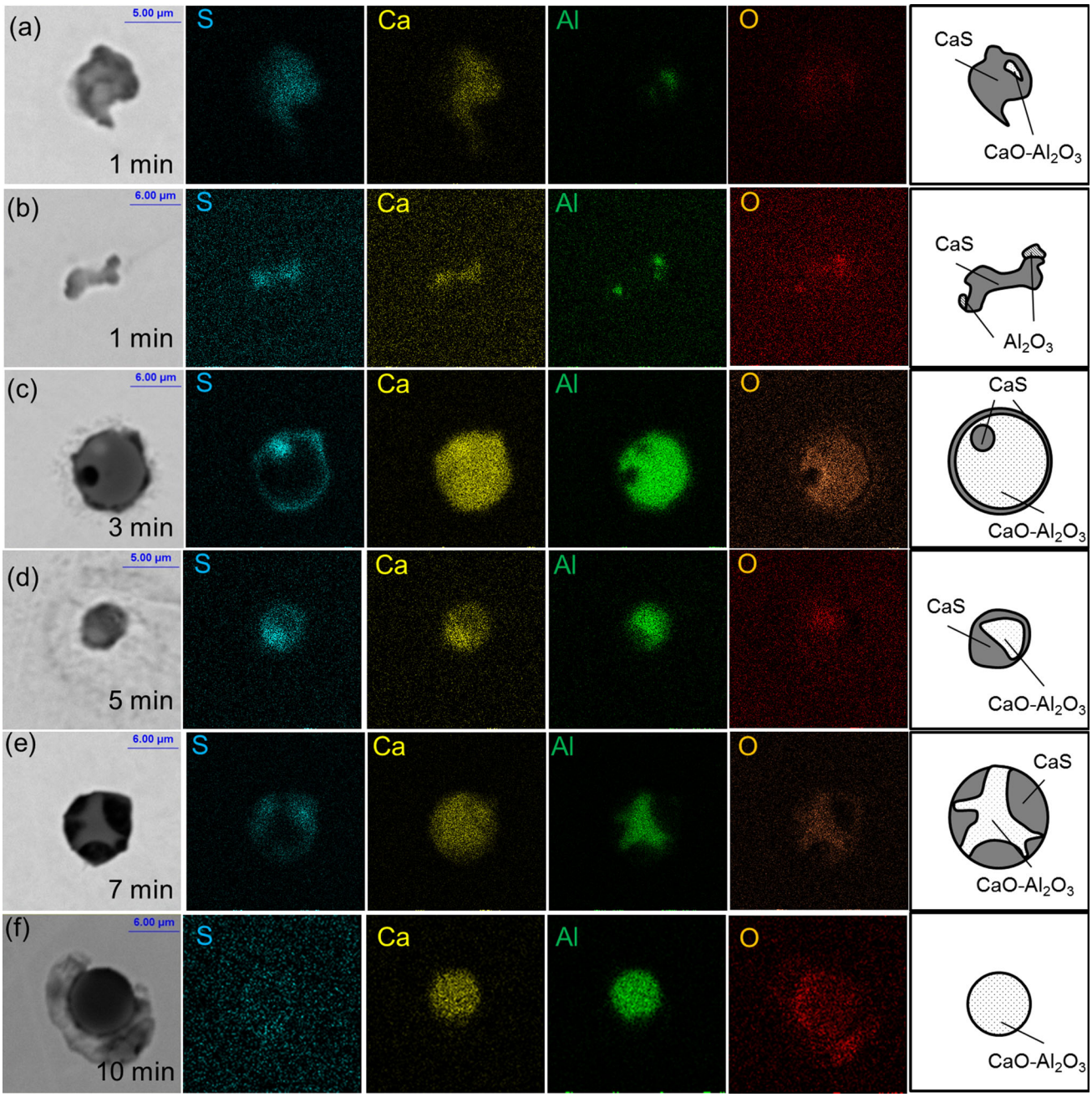

Fig. 8—Typical inclusions in steel with 50 to 90 ppm sulfur: (*a*) CaS-CaO-Al_2O_3, (*b*) CaS-Al_2O_3, (*c*) CaO-Al_2O_3 with a CaS ring, (*d*) CaO-Al_2O_3 surrounded by CaS, (*e*) complex CaS-CaO-Al_2O_3, and (*f*) uniform CaO-Al_2O_3.

The Gibbs free energy of a reaction is often used to describe whether one reaction is favored. The reaction occurs if the Gibbs free energy is negative. As shown in Figure 15, the driving force of the reaction decreased with the decrease of sulfur and calcium contents in steel. Hence, the extent of the reaction of CaS with [O] was determined by the dissolved sulfur content in steel. The deviation between the measured and the calculated results using Langmuir adsorption results from this effect. The dependence of the fraction of CaS decomposition on the sulfur content in steel agreed with that of Gibbs free energy of Reaction [3], as shown in Figure 15.[18,50]

$$(\mathrm{CaO}) + [\mathrm{S}] = (\mathrm{CaS}) + [\mathrm{O}]; \quad \Delta G^{\theta} = 114,521 - 29.8T \qquad [6]$$

$$\Delta G_{\mathrm{r}} = \Delta G^{\theta} + RT \ln Q_{\mathrm{r}} \qquad [7]$$

$$Q_{\mathrm{r}} = a_{\mathrm{CaS}} \cdot f_{\mathrm{O}} \cdot [\mathrm{pct\ O}] / (a_{\mathrm{CaO}} \cdot f_{\mathrm{S}} \cdot [\mathrm{pct\ S}]) \qquad [8]$$

Based on the preceding discussion, a mechanism for the formation and decomposition of CaS and CaO

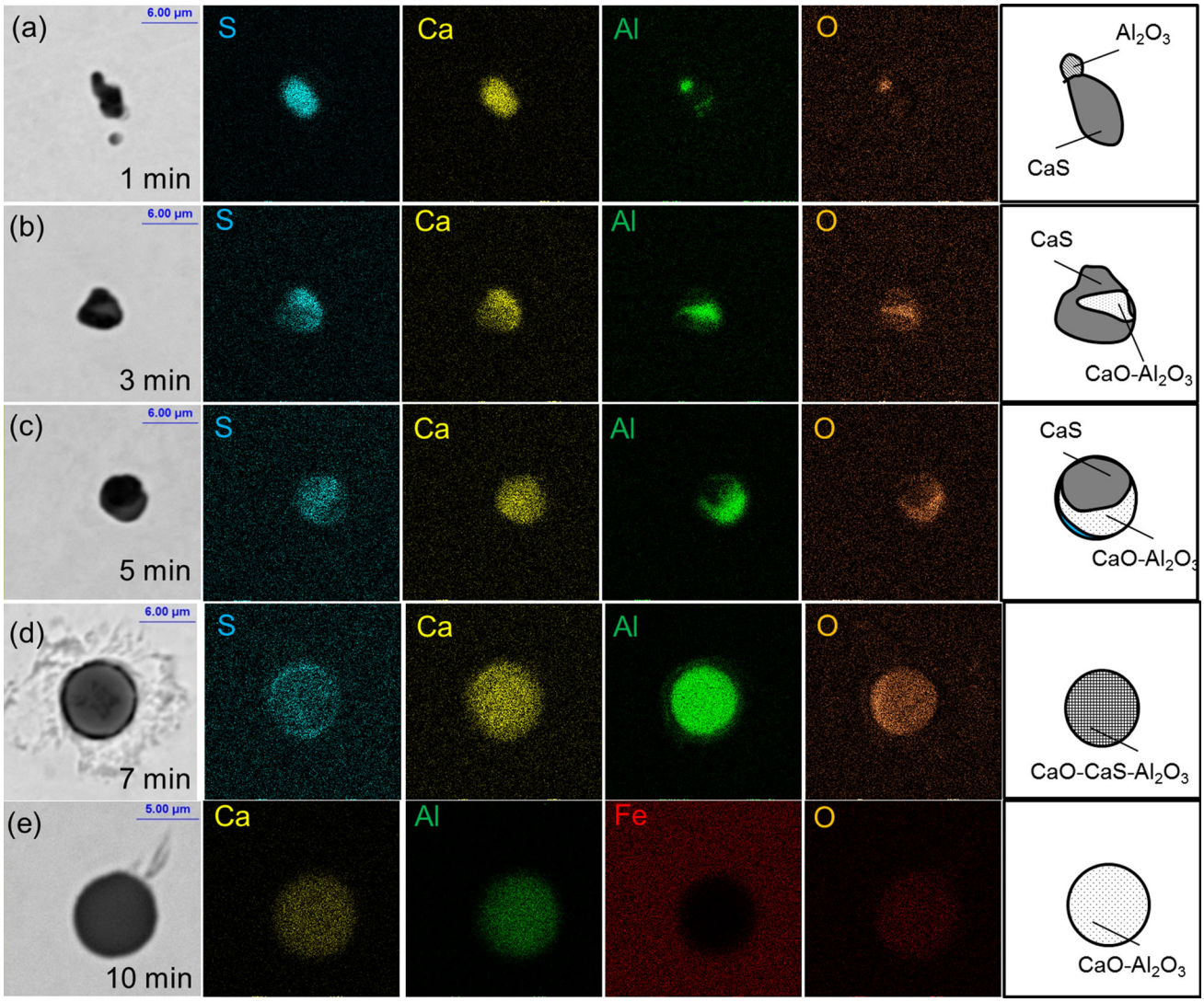

Fig. 9—Typical inclusions in steel with 180 ppm sulfur: (*a*) CaS-Al_2O_3, (*b*) CaO-Al_2O_3 surrounded by CaS, (*c*) complex CaS-CaO-Al_2O_3, (*d*) uniform CaS-CaO-Al_2O_3, and (*e*) uniform CaO·Al_2O_3.

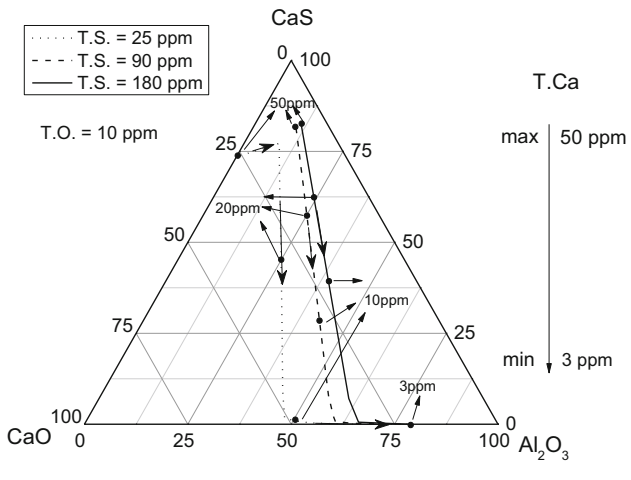

Fig. 10—Composition variation of inclusions with calcium and sulfur contents in steel (calculated with Factsage 7.0 software).

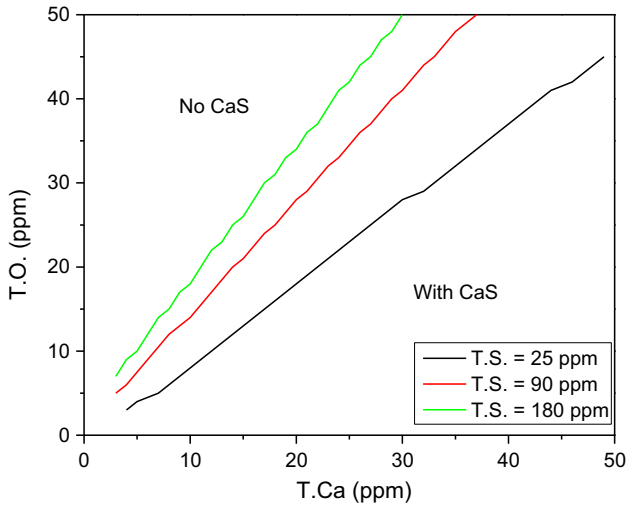

Fig. 11—Critical conditions for the formation of CaS.

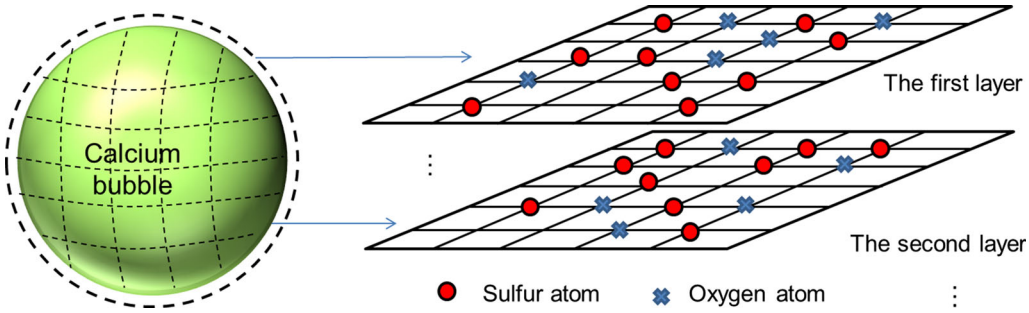

Fig. 12—Reaction model for the formation of CaO and CaS.

Table III. Contents of Calcium, Oxygen, and Sulfur in Detected CaO and CaS, Calculated from Measured Results of Aspex (ppm)

		$Ca_{in\ inclusions}$	$Ca_{in\ CaO}$	$Ca_{in\ CaS}$	$O_{in\ CaO}$	$S_{in\ CaS}$	S/(S + O)
S = 25 ppm heat A	1st sample	6.41	4.40	2.01	1.76	1.61	0.31
S = 50 ppm heat B	1st sample	14.31	7.38	6.39	2.95	5.54	0.48
S = 90 ppm heat C	1st sample	3.75	1.34	2.41	0.54	1.93	0.64
S = 180 ppm heat D	1st sample	15.53	5.14	10.39	2.06	8.34	0.67
S = 180 ppm heat E	1st sample	11.74	3.29	8.45	1.32	6.79	0.72

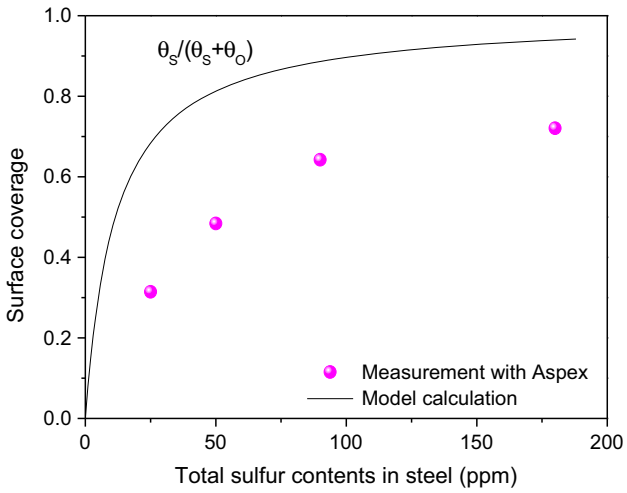

Fig. 13—Dependence of surface coverage on the T.S. in steel.

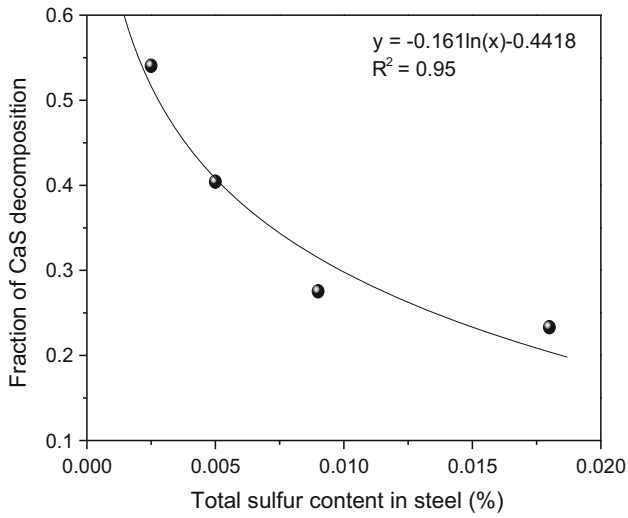

Fig. 14—Relationship between the T.S. content in steel and the fraction of CaS decomposition.

inclusions just after calcium treatment was proposed, as shown in Figure 16. According to the Langmuir adsorption model, CaO and CaS molecules form when solute elements oxygen and sulfur in the molten steel are adsorbed on the surface layer of calcium bubbles. CaS and CaO-CaS became detectable by the agglomeration of smaller CaS and CaO particles. Similarly, the formation of CaS-Al_2O_3 and CaS-CaO-Al_2O_3 occurred by the agglomeration of CaS, Al_2O_3, and CaO particles, as shown in Figure 16(a). Meanwhile, the reaction between CaS and [O] occurred so that CaO-CaS complex inclusions were formed, as illustrated in Figure 16(b). Corresponding transient inclusions, which were measured at the 1-minute sample in heat E, are shown in Figure 17. Based on the composition mapping of inclusions, CaO-CaS was observed in the corner of the CaS inclusion or on the surface of the CaS matrix.

Table IV. First-Order and Second-Order Interaction Coefficients at 1873 K (1600 °C) Used in the Current Work[48,49]

j	Al	Ca	S	O
e_O^j	− 1.17	− 515	− 0.174	− 0.2
e_{Al}^j	0.043	− 0.047	0.035	− 1.98
e_{Ca}^j	− 0.072	− 0.002	− 140	− 780
e_S^j	0.041	− 110	− 0.046	− 0.27

$\gamma_{Ca}^{O} = 6.5 \times 10^5$.

$\gamma_{O}^{Ca} = -1.8 \times 10^4$

$\gamma_{O}^{O,Ca} = 5.2 \times 10^5$

$\gamma_{Ca}^{Ca,O} = -9 \times 10^4$

The reaction between CaS and [O] explained the deviation between the measured result and the calculated result using the Langmuir adsorption model.

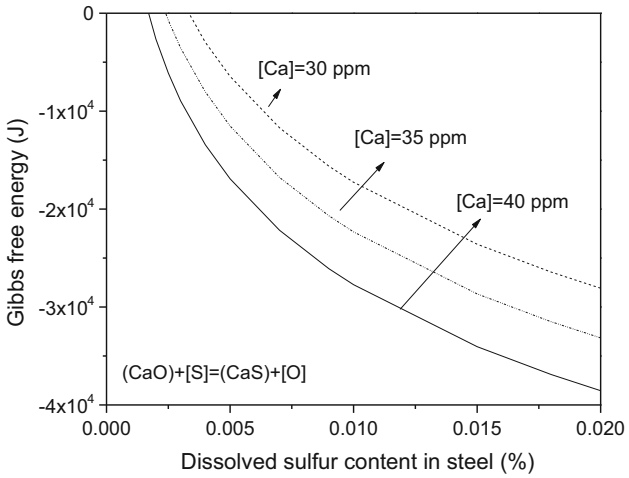

Fig. 15—Relationship between the dissolved sulfur content and the Gibbs free energy for the reaction (CaO) + [S] = (CaS) + [O].

V. EVOLUTION MECHANISM OF CALCIUM SULFIDE

The CaS inclusions are an intermediate reaction product and play an important role for the subsequent modification of alumina inclusions.[30,31,33] The reaction responsible for the modification of alumina is given by[18,50,51]

$$3(\mathrm{CaS}) + (\mathrm{Al_2O_3}) = 3(\mathrm{CaO}) + 2[\mathrm{Al}] + 3[\mathrm{S}]; \quad \Delta G^{\theta} = 520,807 - 133.1T \qquad [9]$$

$$\Delta G_{\mathrm{r}} = \Delta G^{\theta} + RT\ln\left(\frac{a_{\mathrm{CaO}}^{3} f_{\mathrm{Al}}^{2}[\mathrm{Al}]^{2} f_{\mathrm{S}}^{3}[\mathrm{S}]^{3}}{a_{\mathrm{CaS}}^{3} a_{\mathrm{Al_2O_3}}}\right) \qquad [10]$$

Activity coefficients of Al and S used for calculations are listed in Table IV. The activity of Al_2O_3 and CaO in calcium alumina was calculated with Factsage 7.0 software, as shown in Figure 18. Hence, the dependence of the mass fraction of Al_2O_3 in calcium alumina inclusions on the sulfur content in steel was obtained when the Gibbs free energy of the reaction was zero, as illustrated in Figure 19. The figure indicates that the

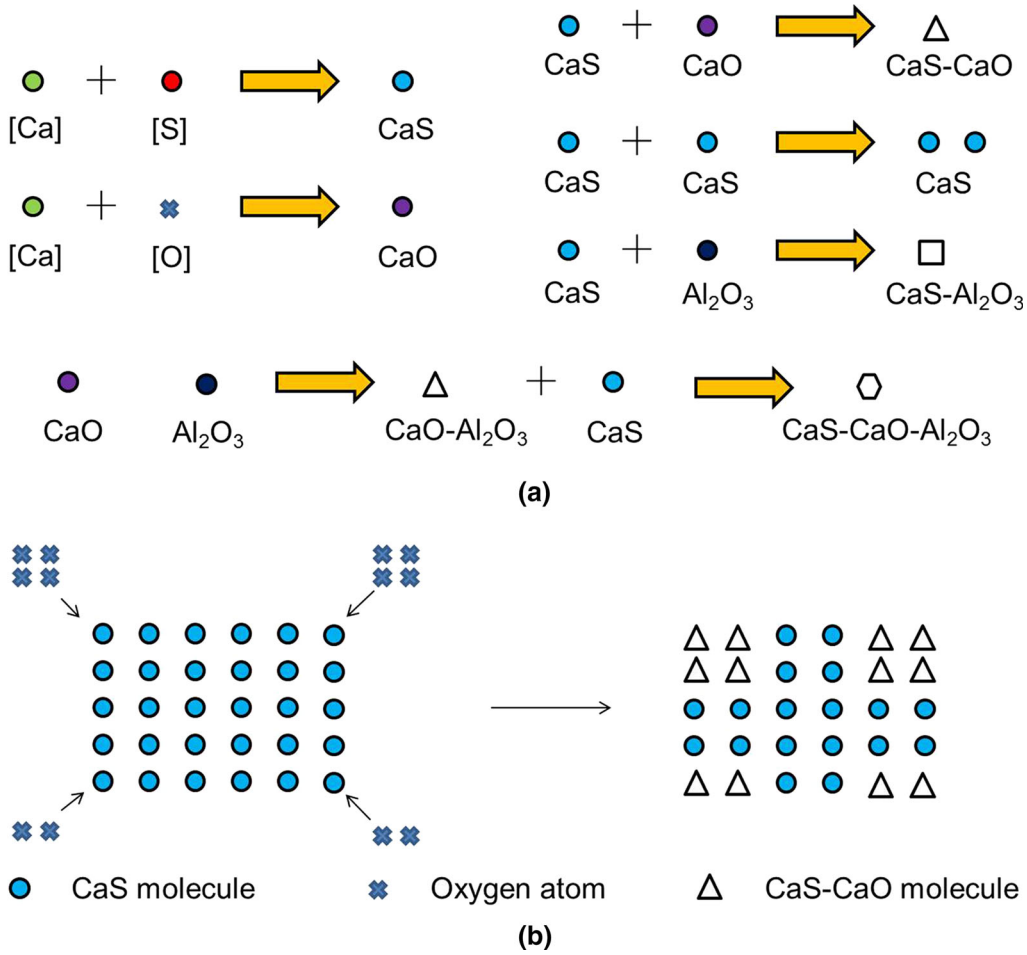

Fig. 16—Mechanism for the formation and the decomposition of CaS and CaO inclusions just after the addition of calcium to the steel: (*a*) formation of inclusions containing CaS and (*b*) reaction between CaS and [O].

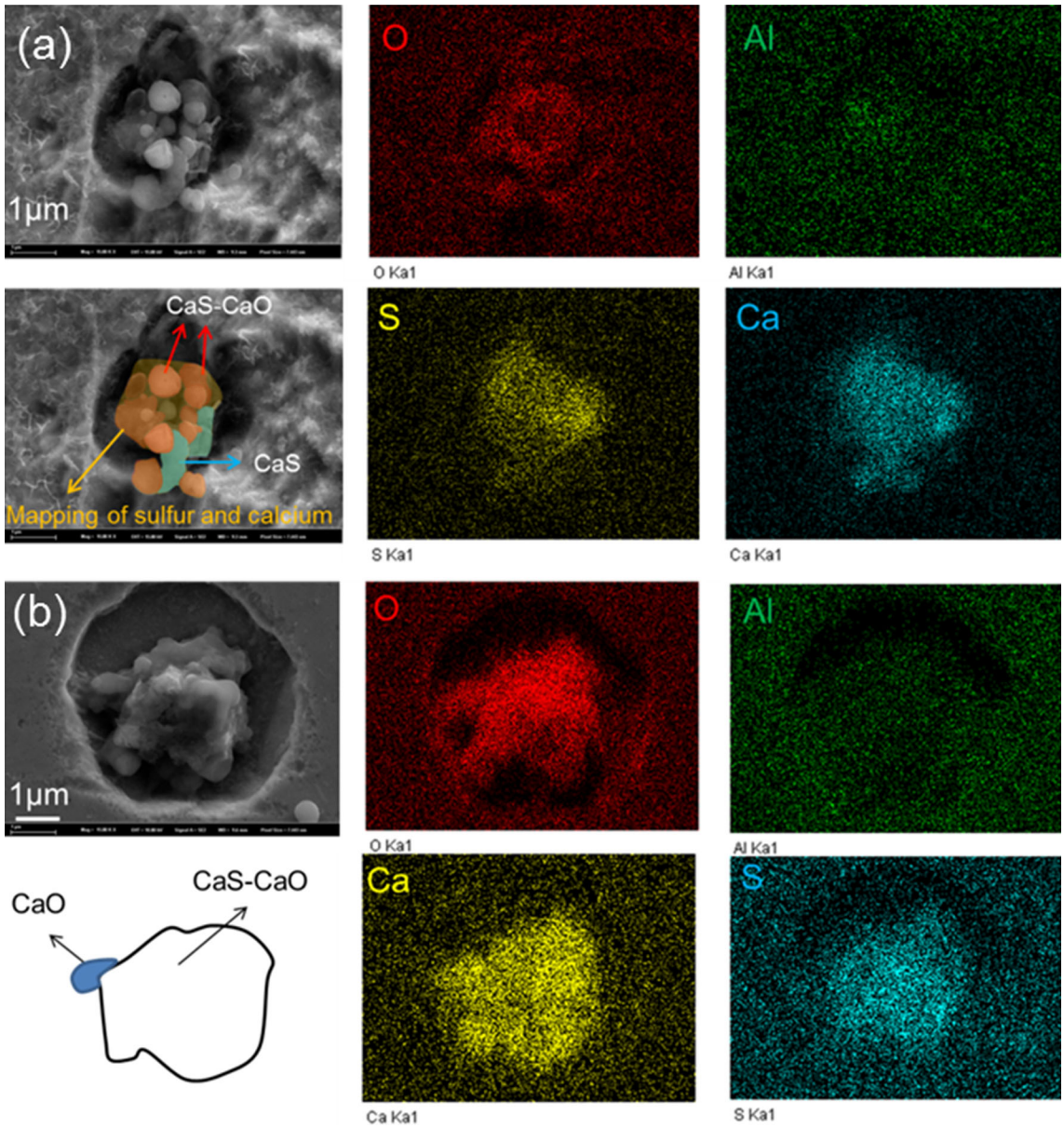

Fig. 17—Composition mappings of transient inclusions formed due to the reaction between CaS and [O]: (*a*) CaS and CaS-CaO inclusions and (*b*) CaO and CaS-CaO inclusions.

modification of alumina was favored if the steel contained low sulfur, and a higher Al_2O_3 content existed in calcium alumina inclusions if the sulfur content in steel increased.

Based on two-dimensional composition mappings of inclusions, the morphology of typical inclusions containing CaS is schematically shown and summarized in Figure 20. Nine stages are defined according to the measured sulfur and calcium contents in steel samples. Different types of dominated inclusions show different patterns at each stage. When sulfur in steel was as low as 25 ppm, CaS mostly adhered to CaO-Al_2O_3 or Al_2O_3 to form a dual-phased inclusion just after the addition of calcium. With decreasing calcium content in steel, inclusions were mostly transferred to globular CaO-Al_2O_3 ones containing a little amount of CaS. When the sulfur content in steel ranged from 50 to 90 ppm, the main type of inclusions contained a core of Al_2O_3 or CaO-Al_2O_3 and the inclusions were completely or partially surrounded by CaS. When the calcium content in steel decreased, the inclusions were mostly uniform CaO-Al_2O_3, CaS-Al_2O_3 complex ones or dual-phased ones of CaO-Al_2O_3 and CaS. With a further decrease of calcium content, inclusions shifted to uniform CaO-Al_2O_3 and dual-phased inclusions of CaO-Al_2O_3 and CaS. When the sulfur content in steel was increased to 180 ppm, dual-phased inclusions of Al_2O_3 and CaS were dominant just after the addition of calcium. Similar tendency for the evolution of inclusions was observed when the sulfur content in steel was higher than 50 ppm, except that many uniform CaS-CaO-Al_2O_3 inclusions existed in the last tapped sample

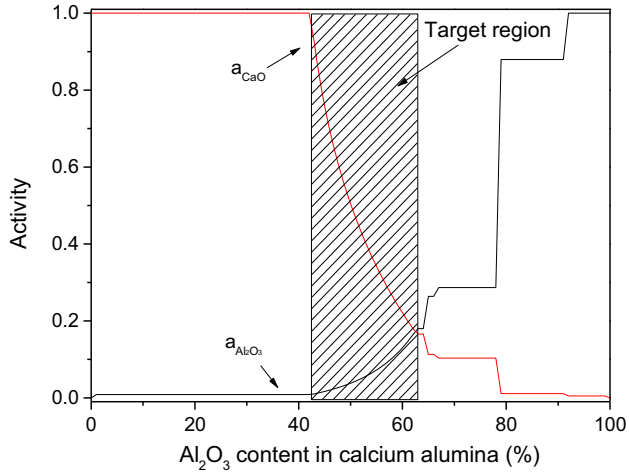

Fig. 18—Activity of Al_2O_3 and CaO in a CaO-Al_2O_3 binary system.

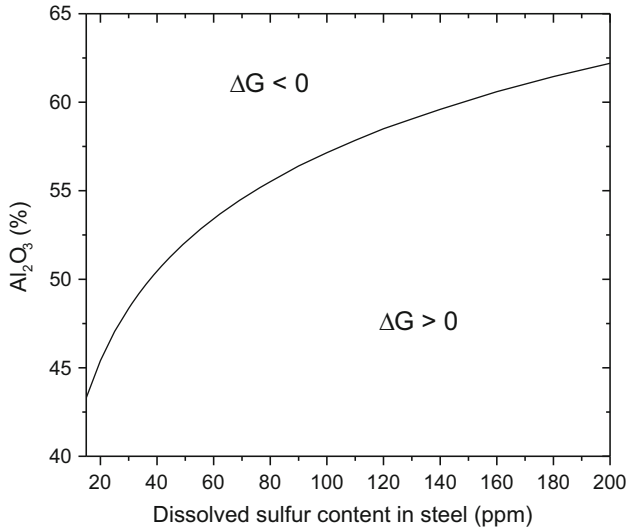

Fig. 19—Relationship between the mass fraction of Al_2O_3 in calcium alumina inclusions and the T.S. content in steel at 1873 K (1600 °C).

for experiments with 180 ppm sulfur in steel. With fixed calcium level, for example, higher than 30 ppm, more inclusions were CaS-Al_2O_3 when the sulfur content in steels was higher than 50 ppm, while inclusions were mostly CaS-Al_2O_3-CaO when the sulfur content was 25 ppm. Sulfur content significantly influenced the morphology of inclusions during calcium treatment.

According to the thermodynamic calculation earlier and the morphology evolution of typical inclusions containing CaS, the variation of transient CaS inclusions could be summarized. In heat A, limited by the sulfur content in steel, CaO-Al_2O_3 and CaO-Al_2O_3-CaS inclusions and a certain amount of CaS-Al_2O_3 formed at first. The evaporation of calcium and the modification reaction between CaS and Al_2O_3 were the two possible influencing parameters responsible for the decomposition of CaS. The modification reaction between CaS and Al_2O_3 was favored in steel with low sulfur, as shown in Figure 19. Hence, CaS-Al_2O_3 inclusions were transferred to CaO-Al_2O_3-(CaS) rapidly. When the sulfur content in steel increased, calcium was mostly captured in CaS so that less CaO was formed just after the addition of calcium. The decomposition of CaS inclusions highly depended on the evaporation of calcium. The reaction between CaS and alumina in steel with increased sulfur, especially in heats D and E, also occurred to generate uniform CaS-CaO-Al_2O_3 inclusions, while the reaction was less intense than that in steel with 25 ppm sulfur. Thus, at the last tapped sample, inclusions were transferred to uniform CaS-CaO-Al_2O_3 inclusions with a high Al_2O_3 content and to dual-phased inclusions of CaS and CaO-Al_2O_3. Increasing sulfur content from 50 to 180 ppm in steel had an influence on the modification of alumina, while the extent of the modification reaction on alumina was limited by the sulfur content in steel. Initially generated CaS inclusions were mostly decomposed due to the evaporation of calcium. The current study concluded that calcium addition involved more the formation of the immediate product CaO, and then the modification occurred by the direct reaction between CaO and

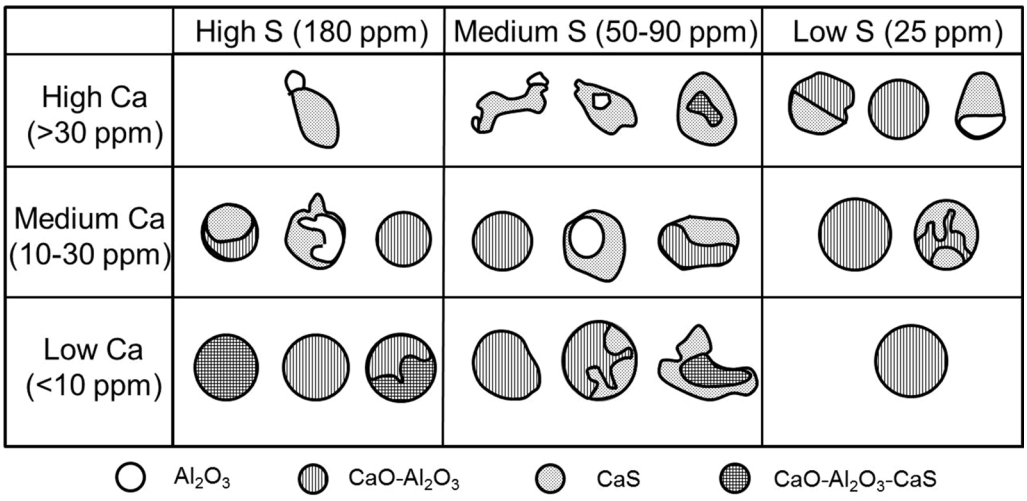

Fig. 20—Typical inclusions in steel samples with different contents of sulfur and calcium.

Al_2O_3.[52] CaO existed stably after the formation of calcium alumina despite the decrease of the calcium content in steel.

VI. CONCLUSIONS

In the current study, the effect of sulfur content in the molten steel on the transient evolution of inclusions was investigated *via* laboratory experiments. Thermodynamic calculation was performed to predict the evolution tendency of the composition of inclusions. A reaction model was proposed for the formation of CaO and CaS, and the variation of transient CaS inclusions was discussed based on the thermodynamic calculation and the morphology evolution of typical inclusions containing CaS. The following conclusions are derived.

1. Sulfur content in steel had an obvious effect on the composition of inclusions during calcium treatment. When the content of sulfur in steel was as low as 25 ppm, the evolution path of inclusions was from CaS-Al_2O_3-CaO to Al_2O_3-CaO-(CaS) with the decrease of calcium in steel. With increasing sulfur content in steel from 90 to 180 ppm, inclusions shifted from CaS-Al_2O_3 to dual-phased ones of CaS and CaO-Al_2O_3 and uniform Al_2O_3-CaO-CaS ones with high Al_2O_3 content.
2. The formation of CaS highly depended on oxygen, calcium, and sulfur contents in steel. The formation of CaS-CaO-Al_2O_3 inclusions with a high Al_2O_3 content was favored in steel with high sulfur content.
3. A reaction model was proposed for the formation of CaO and CaS just after the addition of Ca-Si powders, which was validated by the measurement. The deviation between the measured and calculated results using the Langmuir adsorption model existed since the reaction between CaS and [O] occurred.
4. The decomposition of CaS in Al_2O_3-rich inclusions was favored in steel with a low sulfur content during calcium treatment. With the increased sulfur content in steel, calcium was mostly captured in CaS. Initially generated CaS inclusions were mostly decomposed due to the evaporation of calcium, while the extent of the modification reaction on alumina was limited by the increased sulfur content in steel. Hence, inclusions were mostly uniform CaS-CaO-Al_2O_3 with a high Al_2O_3 content, as well as dual-phased inclusions of CaS and CaO-Al_2O_3 in steel with an increased sulfur content.

ACKNOWLEDGMENTS

The authors are grateful for support from the National Key R&D Program of China (2017YFB0304000 and 2017YFB0304001), the National Science Foundation of China (Grant Nos. 51725402, 51504020, and 51704018), the Fundamental Research Funds for the Central Universities (Grant Nos. FRF-TP-15-001C2, FRF-TP-15-067A1, and FRF-TP-17-039A1), the Guangxi Key Research and Development Plan (Grant No. AB17129006), the National Postdoctoral Program for Innovative Talents (Grant No. BX201700028), and the Beijing Key Laboratory of Green Recycling and Extraction of Metals (GREM) and the High Quality Steel Consortium (HQSC) and Green Process Metallurgy and Modeling (GPM^2), School of Metallurgical and Ecological Engineering, University of Science and Technology Beijing (USTB).

REFERENCES

1. G. Ye, P. Jonsson, and T. Lund: *ISIJ Int*., 1996, vol. 36, pp. S105–S108.
2. N. Verma, M. Lind, P. Pistorius, R. Fruehan, and M. Potter: *Iron Steel Technol*., 2010, vol. 7, pp. 189–97.
3. S. Abdelaziz, G. Megahed, I. Elmahallawi, and H. Ahmed: *Ironmak. Steelmak*., 2009, vol. 36, pp. 432–41.
4. L. Holappa, M. Hamalainen, M. Liukkonen, and M. Lind: *Ironmak. Steelmak*., 2003, vol. 30, pp. 111–15.
5. M. Numata and Y. Higuchi: *ISIJ Int*., 2012, vol. 52, pp. 2013–18.
6. Y. I. Ito, M. Suda, Y. Kato, H. Nakato, and K. I. Sorimachi: *ISIJ Int*., 1996, vol. 36, pp. S148–S150.
7. T. Ikeda, N. Fujino, and H. Ichihashi: *Tetsu-to-Hagané*, 1980, vol. 66, pp. 2040–49.
8. C. E. Cicutti, J. Madias, and J. C. Gonzalez: *Ironmak. Steelmak*., 1997, vol. 24, pp. 155–59.
9. J. Yang, B. T. Chen, T. Wei, F. Z. Zeng, Y. Gang, and S. Feng: *Steel Res. Int*., 2013, vol. 84, pp. 703–12.
10. V. Presern, B. Korousic, and J. W. Hastie: *Steel Res. Int*., 1991, vol. 62, pp. 289–95.
11. H. M. Pielet and D. Bhattacharya: *Metall. Mater. Trans. B*, 1984, vol. 15B, pp. 547–62.
12. Z. Deng and M. Zhu: *Steel Res. Int*., 2013, vol. 84, pp. 519–25.
13. J. M. A. Geldenhuis and P. C. Pistorius: *Ironmak. Steelmak*., 2000, vol. 27, pp. 442–49.
14. G. Yang and X. Wang: *ISIJ Int*., 2015, vol. 55, pp. 126–33.
15. W. V. Bielefeldt and A. C. F. Vilela: *Steel Res. Int*., 2015, vol. 86, pp. 375–85.
16. Y. Kusano, Y. Kawauchi, M. Wajima, K. Sugawara, M. Yoshida, and H. Hayashi: *ISIJ Int*., 1996, vol. 36, pp. S77–S80.
17. G. Yang, X. Wang, F. Huang, P. Wei, and X. Hao: *Metall. Mater. Trans. B*, 2015, vol. 46B, pp. 145–54.
18. K. Taguchi, O. N. Hideki, D. Nakai, T. Usui, and K. Marukawa: *ISIJ Int*., 2003, vol. 43, pp. 1705–09.
19. T. Ototani, Y. Kataura, and T. Degawa: *Tetsu-to-Hagané*, 1975, vol. 61, pp. 2167–81.
20. S. Seetharaman, A. McLean, R. Guthrie, and S. Sridhar: *Treatise on Process Metallurgy*, 1st ed., Elsevier, Amsterdam, 2013, pp. 353–58.
21. D. C. Hilty and V. T. Popp: *Proc. Electric Furnace Conf*., 1969, vol. 27, pp. 52–66.
22. H. Gaye, P. Rocabois, J. Lehman, and M. Wintz: *McLean Symposium Proceedings*, 1998, pp. 67–76.
23. D. Janke, Z. Ma, P. Valentin, and A. Heinen: *ISIJ Int*., 2000, vol. 40, pp. 31–39.
24. K. Larsen and R. J. Fruehan: *Iron Steelmaker*, 1991, vol. 12, pp. 125–32.
25. I. G. Davies and P. C. Morgan: *Ironmak. Steelmak*., 1985, vol. 12, pp. 176–84.
26. C. Gatellier, H. Gaye, J. Lehmann, and Y. Zbaczyniak: *Rev. Metall. CIT*, 1992, vol. 89, pp. 887–88.
27. W. Yang, L. Zhang, X. Wang, Y. Ren, X. Liu, and Q. Shan: *ISIJ Int*., 2013, vol. 53, pp. 1401–10.
28. G. Xu, Z. Jiang, and Y. Li: *Metall. Mater. Trans. B*, 2016, vol. 47B, pp. 2411–20.
29. D. Z. Lu, G. A. Irons, and W. K. Lu: *Ironmak. Steelmak*., 1994, vol. 21, pp. 362–71.

30. N. Verma, P. C. Pistorius, R. J. Fruehan, M. Potter, M. Lind, and S. Story: *Metall. Mater. Trans. B*, 2011, vol. 42B, pp. 711–19.
31. Y. Ren, L. Zhang, and S. Li: *ISIJ Int.*, 2014, vol. 54, pp. 2772–79.
32. Y. Higuchi, M. Numata, S. Fukagawa, and K. Shinme: *ISIJ Int.*, 1996, vol. 36, pp. S151–S154.
33. N. Verma, P. C. Pistorius, R. J. Fruehan, M. Potter, M. Lind, and S. R. Story: *Metall. Mater. Trans. B*, 2011, vol. 42B, pp. 720–29.
34. N. Verma, P. C. Pistorius, R. J. Fruehan, M. S. Potter, H. G. Oltmann, and E. B. Pretorius: *Metall. Mater. Trans. B*, 2012, vol. 43B, pp. 830–40.
35. J. Xu, F. Huang, and X. Wang: *Metall. Mater. Trans. B*, 2016, vol. 47B, pp. 1217–27.
36. Y. T. Guo, S. P. He, G. J. Chen, and Q. Wang: *Metall. Mater. Trans. B*, 2016, vol. 47B, pp. 2549–57.
37. W. Tiekink, B. Santillana, R. Boom, R. Kooter, F. Mensonides, and B. Deo: *Iron Steel Technol.*, 2008, vol. 5, pp. 184–95.
38. X. Wang, F. Huang, L. Qiang, L. Haibo, and Y. Jian: *Steel Res. Int.*, 2014, vol. 85, pp. 155–63.
39. S. K. Choudhary and A. Ghosh: *ISIJ Int.*, 2008, vol. 48, pp. 1552–59.
40. Y. Wang, M. Valdez, and S. Sridhar: *Metall. Mater. Trans. B*, 2002, vol. 33B, pp. 625–32.
41. D. Z. Lu, G. A. Irons, and W. K. Lu: *Ironmak. Steelmak.*, 1991, vol. 18, pp. 342–47.
42. C. H. Leung and L. H. V. Vlack: *Metall. Mater. Trans. A*, 1981, vol. 12A, pp. 987–91.
43. R. Piao, H. G. Lee, and Y. B. Kang: *ISIJ Int.*, 2013, vol. 53, pp. 2132–41.
44. L. Zhang, Y. Liu, Y. Zhang, Y. Ren, W. Yang, and W. Chen: Unpublished research, University of Science and Technology Beijing, 2017.
45. G. R. Belton and R. W. Hunt: *Metall. Mater. Trans. B*, 1993, vol. 24B, pp. 241–58.
46. G. R. Belton: *Metall. Mater. Trans. B*, 1976, vol. 7B, pp. 35–42.
47. W. Tiekink, R. V. D. Bogert, T. Breedijk, and A. Ferguson: *Ironmak. Steelmak.*, 2003, vol. 30, pp. 146–50.
48. Y. Kagan and I. S. Lyubutin: *Steelmaking Data Sourcebook*, Revisedst ed., Gordon and Breach Science Publishers, New York, NY, 1988.
49. M. Hino and K. Ito: *Thermodynamic Data for Steelmaking*, Tohoku University Press, Sendai, 2010, p. 171.
50. M. Hino and K. Itoh: *Recommended Values of Equilibrium Constants for the Reactions in Steelmaking*, Japan Society for the Promotion of Science, Tokyo, 1984.
51. H. Itoh, M. Hino, and S. Ban-Ya: *Metall. Mater. Trans. B*, 1997, vol. 28B, pp. 953–56.
52. M. Lind and L. Holappa: *Metall. Mater. Trans. B*, 2010, vol. 41B, pp. 359–66.